Eur Biophys J (2008) 37:1065–1071
DOI 10.1007/s00249-008-0298-8

BIOPHYSICS LETTER

Modulation of the conductance of a 2,2′-bipyridine-functionalized peptidic ion channel by Ni^{2+}

Claudia S. Pilz · Claudia Steinem

Received: 14 November 2007 / Revised: 22 February 2008 / Accepted: 26 February 2008 / Published online: 18 March 2008

Abstract An α-helical amphipathic peptide with the sequence H_2N-$(LSSLLSL)_3$-$CONH_2$ was obtained by solid phase synthesis and a 2,2′-bipyridine was coupled to its N-terminus, which allows complexation of Ni^{2+}. Complexation of the 2,2′-bipyridine residues was proven by UV/Vis spectroscopy. The peptide helices were inserted into lipid bilayers (nano black lipid membranes, nano-BLMs) that suspend the pores of porous alumina substrates with a pore diameter of 60 nm by applying a potential difference. From single channel recordings, we were able to distinguish four distinct conductance states, which we attribute to an increasing number of peptide helices participating in the conducting helix bundle. Addition of Ni^{2+} in micromolar concentrations altered the conductance behaviour of the formed ion channels in nano-BLMs considerably. The first two conductance states appear much more prominent demonstrating that the complexation of bipyridine by Ni^{2+} results in a considerable confinement of the observed multiple conductance states. However, the conductance levels were independent of the presence of Ni^{2+}. Moreover, from a detailed analysis of the open lifetimes of the channels, we conclude that the complexation of Ni^{2+} diminishes the frequency of channel events with larger open times.

Keywords Helix bundle · Lipid bilayer · Nano-BLMs · Peptide assembly · Single channel recordings

Introduction

Two structural motifs of ion channels are found in nature, one based on transmembrane amphipathic α-helical peptides forming a hydrophilic pore (Unwin 2003), whereas the other one is characterized by β-barrels as is found in porines (Buchanan 1999). A wealth of information about ion channels has been gathered from the assembly of simple α-helical peptides in lipid bilayers. The most well-known example is the peptaibol alamethicin, an antibiotic from *Trichoderma viride*, which forms voltage-gated ion channels with multiple conductance levels. This behaviour can be explained by the formation of transmembrane aggregates (Milov et al. 2007) according to the barrel stave mechanism. The uptake and release of alamethicin helical monomers from a channel aggregate accounts for the observed multi-state conductance levels (Cafiso 1994). These multi-state conductance levels were monitored not only in classical black lipid membranes (BLMs) but also in nano-BLMs, recently introduced by our group (Römer and Steinem 2004). Nano-BLMs are produced on highly ordered porous substrates providing a high long-term and mechanical stability, while both membrane leaflets are still accessible and membrane potentials can be applied allowing for single channel recordings of peptides such as gramicidin and alamethicin and large proteins such as OmpF from *Escherichia coli* (Römer et al. 2004; Römer and Steinem 2004; Schmitt et al. 2006). To modulate and control such conductance states, Mutter and coworkers have introduced the concept of template assembled synthetic proteins (TASP), in which peptide helices are covalently linked to a

Electronic supplementary material The online version of this article (doi:10.1007/s00249-008-0298-8) contains supplementary material, which is available to authorized users.

C. S. Pilz · C. Steinem (✉)
Institut für Organische und Biomolekulare Chemie,
Georg-August Universität, Tammannstr. 2,
37077 Göttingen, Germany
e-mail: claudia.steinem@chemie.uni-goettingen.de

template resulting in a well defined helix bundle (Mutter and Vuilleumier 1989). This method has been applied by others demonstrating that indeed defined conductance states are formed (Becker et al. 2004; Duclohier et al. 2003; Montal et al. 1990, 1993). Modulation of open lifetimes of peptide channels was observed by Asami and coworkers (Sakoh et al. 2003), who covalently bridged two alamethicin molecules via a disulfide bond resulting in prolonged open lifetimes presumably as a result of a reduced lateral diffusion of the peptides.

Here, we synthesized an α-helical amphipathic peptide to which a bipyridine moiety was attached in order to answer the question how the conductance behaviour of the peptide is altered by complexation of the bipyridine residues with Ni^{2+}. The synthetic peptide sequence H_2N-(LSSLLSL)$_3$$CONH_2$ (Lear et al. 1988) itself has already been shown to insert into lipid bilayers as an amphipathic α-helix, forming cation selective ion channels with an effective diameter of 0.8 nm under voltage control (Akerfeldt et al. 1993; Chung et al. 1992; Lear et al. 1988). From the effective diameter and computer simulations it is concluded that a hexameric bundle is formed in lipid bilayers (Akerfeldt et al. 1993; Lear et al. 1988; Randa et al. 1999). N-acetylation of the peptide sequence strongly influences the conductance behaviour of the peptide. Kienker and Lear (1995) obtained different conductance states as well as longer open times of the *N*-acetylated peptide compared to the underivatized one.

Here, we attached a bipyridine moiety to the N-terminus of this peptide. Bipyridine is a well-characterized metal acceptor, which is utilized for various supramolecular assemblies including α-helical coiled coil peptides (Gilmartin et al. 2005; Kaes et al. 2000; Koide et al. 2002). Several examples are found in literature, where water soluble peptides are covalently coupled to 2,2′-bipyridine allowing complex formation via metal cations resulting in dimeric and trimeric peptide assemblies (Ghadiri et al. 1992; Gochin et al. 2002, 2003; Liebermann and Sasaki 1991). To our knowledge, bipyridine has not yet been used to modulate the ion channel behaviour of peptide helix bundles in a lipid membrane environment.

Experimentals

Synthesis of H_2N-(LSSLLSL)$_3$-$CONH_2$ (**1**)

The peptide H_2N-(LSSLLSL)$_3$-$CONH_2$ (**1**) was obtained by Fmoc-solid phase synthesis on a TentaGel-S Ram Fmoc resin (0.3 mmol/g) (Advanced ChemTech, Giessen, Germany) using a peptide synthesizer (Advanced ChemTech Model 90). Fmoc-amino acid derivatives (Advanced ChemTech, 3 to 5 equiv.) were coupled twice using HOBt/HBTU/DIEA (3:3:3 up to residue 9, 5:5:10 for the remaining) in DMF for 30–60 min. The Fmoc group was removed by 20% piperidine in DMF up to residue 9 (two times, 15 min each), and 40% (5 min) followed by 20% piperidine in DMF (25 min) for the following residues. The peptide was cleaved from the resin by TFA/triisopropylsilane/H_2O (85:7.5:7.5) for 1 h. After removing TFA, the crude peptide was isolated by cold ether precipitation and purified by HPLC (column: Phenomenex Luna C18(2), 21.1 × 250 mm^2; gradient: 10–75% A in 50 min, 75–95% A in 8 min, 95% A; A: acetonitrile; B: 0.1% aqueous TFA; flow rate: 11 mL/min). Yield: 3%. ESI-MS: *m/z*: 2159.4 $[M + H]^+$, 1447.4 $[2M + 2H + Na]^{3+}$, 1439.9 $[2M + 3H]^{3+}$, 1090.9 $[M + H + Na]^{2+}$, 1080.3 $[M + 2H]^{2+}$, 720.3 $[M + 3H]^{3+}$, calcd. for $C_{99}H_{181}N_{22}O_{30}$: 2159.3.

Synthesis of 8-(4′-methyl-2,2′-bipyridine-4-yl)-octanoic acid (**2**)

2 was synthesized in three steps according to Mohler et al. (2002) starting with an alkenylation of 4,4′-dimethyl-2,2′-bipyridine (Sigma-Aldrich, Taufkirchen, Germany) after deprotonation. Monofunctionalization was controlled by the reaction equivalents resulting in a rather low yield of 22%. Ozonolysis in basic methanol (91% yield) followed by the hydrolysis of the obtained ester (85% yield) results in **2**. CI-MS: *m/z*: 313.3 $[M + H]^+$, 299.3 $[M\text{-}CH_2]^+$, calcd. for $C_{19}H_{25}N_2O_2$: 313.2; ^{1}H NMR (400 MHz, $CDCl_3$ δ ppm 8.59 (d, J = 5.1 Hz, 1H), 8.57 (d, J = 5.0 Hz, 1H), 8.25 (br s, 1H), 8.21 (br s, 1H), 7.19 (dd, J = 5.1, 0.9 Hz, 1H), 7.15 (dd, J = 5.0, 1.6 Hz, 1H), 2.71 (t, J = 7.6 Hz, 2H), 2.46 (s, 3H), 2.36 (t, J = 7.2 Hz, 2H), 1.77–1.61 (m, 4H), 1.42–1.35 (m, 6H).

Synthesis of **3**

Activation of **2** was achieved by adding 0.3 mmol pentafluorophenol in 40 µl EtOAc/DMF (1:1) to 0.1 mmol **2** dissolved in 200 µl EtOAc/DMF (1:1). The solution was stirred on an ice bath, while 0.3 mmol *N*,*N*′-diisopropylcarbodiimide was added. The reaction mixture was stirred for 1 h on an ice bath followed by 1 h at room temperature. The product **2a** was precipitated with hexane. ESI-MS: *m/z*: 478.2 $[M]^{\cdot+}$, 295.2 $[M\text{-}C_6F_5O]^{\cdot+}$, 281.2 $[M\text{-}C_{13}H_{13}N_2]^{\cdot+}$, 267.2 $[M\text{-}C_{14}H_{15}N_2]^{\cdot+}$, 197.2 $[M\text{-}C_{12}F_5H_{10}O_2]^{\cdot+}$, 184.1 $[C_6F_5OH]^{\cdot+}$ calcd. for $C_{25}H_{23}N_2O_2F_5$: 478.2.

2a was coupled to the *N*-terminus of **1**. A solution of 1.3 µmol **1** and 4.2 µmol **2a** in 100 µl DMF was stirred on an ice bath. 2 µl DIEA/DMF (1:8) were added and the reaction mixture was stirred for 1 h on an ice bath and then for additional 4 h at room temperature. The product **3** was precipitated with ether and purified by HPLC (column: Phenomenex Luna C18(2), 4.6 × 150 mm^2; gradient:

3–98% A in 30 min, 98% A; A: 2-propanol; B: aqueous 0.0059% TFA; flow rate: 0.4 mL/min. Yield: 38%. ESI-MS: *m/z*: 1238.2 $[M + H + Na]^{2+}$, 1236.2 $[M + H + NH_4]^{2+}$, 1227.6 $[M + 2H]^{2+}$, 833.1 $[M + H + 2Na]^{3+}$, 831.5 $[M + H + 2NH_4]^{3+}$, 826.8 $[M + 2H + Na]^{3+}$, 824.4 $[M + 2H + Na]^{3+}$, 818.7 $[M + 3H]^{3+}$, calculated for $C_{118}H_{202}N_{24}O_{31}$: 2452.5.

UV/Vis-spectroscopy

UV/Vis-absorption spectra of compounds **2** and **3** dissolved in ethanol were obtained in the absence and presence of $NiCl_2$. Spectra were recorded on a Cary 50 Scan UV/Vis-spectrometer (Varian, Darmstadt, Germany) with a quartz glass cuvette and a path length of 1 cm at room temperature.

Nano-BLM formation and peptide insertion

Porous alumina substrates with open pores of 60 nm diameter were prepared and functionalized with 1,2-dipalmitoyl-*sn*-glycero-3-phosphothioethanol (DPPTE, Avanti Polar Lipids, Alabaster, AL, USA) as described elsewhere (Horn and Steinem 2005; Römer and Steinem 2004; Schmitt et al. 2006). The resulting hydrophobic substrates were placed in a Teflon chamber separating two electrolyte-filled compartments. Nano-BLM formation was achieved by applying 8.5 µl of 20 mM 1,2-diphythanoyl-*sn*-glycero-3-phosphocholine (DPhPC, Avanti Polar Lipids) in n-decane. Symmetric electrolyte conditions with 0.5 M KCl in both compartments were used. A small quantity of **3** in ethanol was added to the electrolyte at one side of the membrane (designated as the *cis* side) leading to a final peptide concentration of 0.03–3.75 nM.

Impedance analysis

The electrical properties of nano-BLMs as well as their formation process on the porous substrates were characterized by impedance spectroscopy using the gain/phase analyser SI 1260 and the 1296 Dielectric Interface (Solartron Instruments, Farnborough, UK) controlled by a personal computer using ZPlot 2.8. Membrane formation was observed time-resolved by reading out the absolute value of the impedance $|Z|(f)$ and the phase angle between current and voltage $\phi(f)$ at a constant frequency of 10^6 Hz (Schmitt et al. 2006). Impedance spectra ($|Z|(f)$, $\phi(f)$) were recorded in a frequency range of 10^{-1}–10^6 Hz. Platinized platinum wires served as working and counter electrodes. All data points were obtained at zero offset potential applying an AC voltage of 30 mV. The Solartron Impedance Measurement Software (version 3.5.0) was used for data recording, the software package Zview2.6b with Calc-Modulus data weighting for data analysis.

Single channel recordings

Currents were recorded with an Axopatch 200B amplifier (Axon Instruments, Foster City, CA, USA), filtered with a four-pole, low-pass Bessel filter of 1 kHz and digitized by an A/D converter (Digidata 1322, Axon Instruments) under voltage clamp conditions with a holding potential $U = +200$ mV with respect to the *trans* side (ground). Two Ag/AgCl wires served as electrodes. The sampling rate was 50 kHz. Data recording and analysis was performed using pClamp9.1 (Axon Instruments). Prior to analysis the data were filtered with a 500 Hz low-pass Gaussian filter.

Results and discussion

Based on the peptide sequence (**1**), we attached 8-(4′-methyl-2,2′-bipyridine-4-yl)-octanoic acid (**2**) to the *N*-terminus resulting in the receptor functionalized peptide **3** (Scheme 1) to allow for a modulation of the channel activity by complexation of the 2,2′-bipyridines with Ni^{2+}. To prove whether complex formation in the presence of $NiCl_2$ occurs, UV/Vis-spectra of **2** and **3** were taken in ethanol in the absence and presence of $NiCl_2$. **2** shows two $\pi \rightarrow \pi^*$ absorption bands at 241 and 282 nm, respectively (Fig. 1a). The presence of equimolar concentrations of Ni^{2+} leads to a bathochrome shift associated with a splitting of the band at longer wavelengths. This results in three distinct absorption bands at 250, 294, and 305 nm. The found bathochromic shift of the absorption band with a concomitant band splitting in the presence of a metal cation is characteristic for the formation of a Ni^{2+}-2,2′-bipyridine complex (Gilliam et al. 1941; Mason 1968). In Fig. 1b, the absorption spectrum of **3** dissolved in ethanol in the absence of $NiCl_2$ is shown. Only one maximum at 278 nm is discernable, while the second characteristic $\pi \rightarrow \pi^*$ absorption band at 240 nm is super-

Scheme 1 Synthesis of **3**

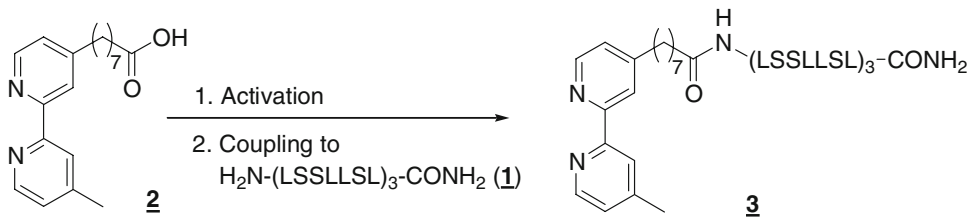

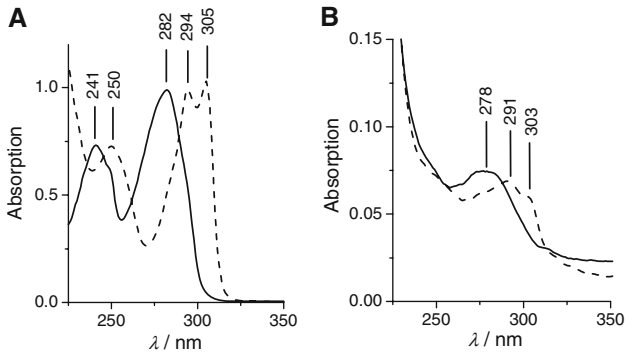

Fig. 1 **a** UV/Vis absorption spectra of 68.2 μM **2** in ethanol in absence (*solid line*) and presence (*dotted line*) of 70 μM $NiCl_2$. **b** UV/Vis absorption spectra of 5.2 μM **3** in ethanol in absence (*solid line*) and presence (*dotted line*) of 13 μM $NiCl_2$

imposed by the absorption band of the peptide bonds. Addition of Ni^{2+} leads to a bathochromic shift, and a splitting into two bands at 291 and 303 nm, which can be attributed to the complexation of the bipyridine functionality by Ni^{2+}.

To investigate the channel activity of **3**, nano-BLMs were used for single-channel recordings. Nano-BLMs have been shown to provide a long term and mechanically stable system with membrane resistances that are sufficiently high to monitor channel events and are thus a more robust alternative to classical BLMs (Horn and Steinem 2005; Römer and Steinem 2004; Schmitt et al. 2006) First attempts to insert the peptide into classical BLMs by adding the peptide from an ethanolic solution resulted only in non-defined current bursts indicating a destabilization of the membrane upon insertion of the peptide. However, insertion of compound **3** in nano-BLMs resulted in well-defined single channel events. We conclude that the functionalized porous substrates underlying the nano-BLMs provide a stability that overcomes the problem of membrane destabilization upon peptide insertion. The hydrophobic anchoring of the membrane on the porous substrate appears to contribute significantly to the overall stability upon peptide insertion. We have carried out a similar observation for the peptide $Vpu_{1–32}$, which was inserted into micro-BLMs supported onto DPPTE-functionalized porous silicon substrates and in membranes attached to porous silicon without functionalization (Römer et al. 2004). Only if the DPPTE-submonolayer was present, well-defined single channel events were observed over a longer period of time.

Nano-BLMs were prepared on porous alumina substrates with pore sizes of 60 nm that were functionalized with gold and 1,2-dipalmitoyl-*sn*-glycero-3-phosphothioethanol. From impedance analysis, the electrical characteristics of the nano-BLMs prepared from 1,2-diphytanoyl-*sn*-glycero-3-phosphocholine were extracted leading to a mean specific membrane capacitance of (0.39 ± 0.03) μF/cm^2 ($n = 22$) and a membrane resistance in the GΩ regime.

First, the ion channel properties of **3** in the absence of Ni^{2+} were characterized by single channel recordings under voltage clamp conditions. **3** was added from an ethanolic solution to the *cis*-compartment in a concentration of 0.03–3.75 nM, while applying a holding potential of +200 mV (referring to the *cis* side). After addition of the peptide, characteristic rectangular current traces were observed (Fig. 2a). We attribute this step-like current increase and decrease to the assembly and disassembly of a helix bundle composed of a defined number of amphipathic peptide helices. Altogether, four different opening levels were discernable in the current range of around 25 pA (O_1), 35 pA (O_2), 45 pA (O_3) and 70 pA (O_4). Channel events of one opening level were often observed in bursts, which lasted several seconds. The majority of all observed channel events were found in the range of 15–110 pA. To quantitatively evaluate the conductance levels, a conductance histogram analysis was performed. All events that were characterized by a current plateau were taken as channel events. Conductances were calculated from the current traces taking the applied voltage of +200 mV into account. Figure 2c shows the obtained histogram up to a conductance of 600 pS including 3,556 events. Four Gaussian functions were fitted to the data resulting in four distinct conductance states with $G_1 = (131 \pm 19)$ pS, $G_2 = (181 \pm 20)$ pS, $G_3 = (234 \pm 20)$ pS, and $G_4 = (374 \pm 70)$ pS. 968 events were found to exhibit a conductance state above 600 pS, which is 21% of all events that were read out (see supplementary material). Taking the fact that the lowest conductance state is a result of six peptide monomers forming a helix bundle, like it is proposed by DeGrado and coworkers (Akerfeldt et al. 1993; Lear et al. 1988), the higher conductance states would be a result of a continuous increase in the number of helices participating in the bundle up to nine helices. Similarly, we have found five different conductance states of alamethicin in nano-BLMs in 0.5 M KCl exhibiting conductance levels ranging from 200 to 6,000 pS (Römer and Steinem 2004). The different observed conductance states are attributed to helix bundles composed of different numbers of alamethicin monomers, ranging from 4 up to 11 (Sansom 1991).

We asked the question, how the presence of Ni^{2+} resulting in the complexation of the 2,2′-bipyridine-ligands might alter the channel properties of **3**. Prior the addition of $NiCl_2$, the incorporation of the peptide into nano-BLMs was confirmed by the appearance of channel events with the characteristics as shown in Fig. 2a. After single channels were monitored, $NiCl_2$ in a concentration of 2.5–5 μM was added to both sides. Again, characteristic current traces were observed in presence of Ni^{2+}, and the majority of events were found in a current range of 15–110 pA (Fig. 2b). Channel events were observed mainly in bursts with one distinct current level. To quantitatively evaluate the conductance states, a histogram analysis of 2,189 events

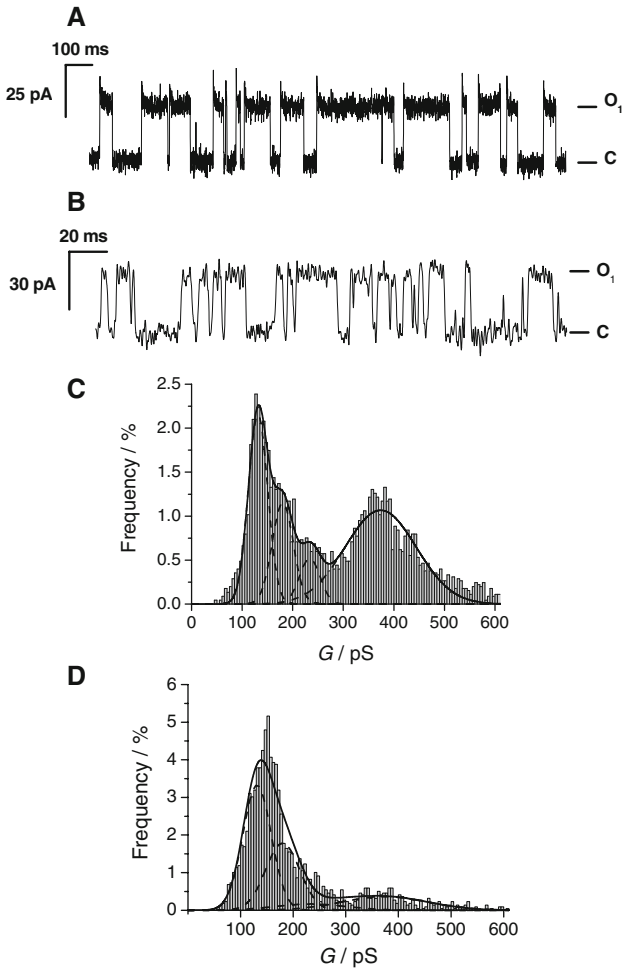

Fig. 2 Channel recordings of **3** in nano-BLMs. **a** Characteristic current trace (channel opens upwards) of **3** obtained at +200 mV in 0.5 M KCl in the absence of $NiCl_2$. **b** Characteristic current trace (channel opens upwards) of **3** obtained at +200 mV in 0.5 M KCl in the presence of $NiCl_2$. **c** Histogram analysis of the observed conductance states of **3** in nano-BLMs up to 600 pS [3,556 events, bin width: 5 pS, normalized to all events (4,524)] in the absence of $NiCl_2$. **d** Histogram analysis of the conductance states of **3** in the presence of 2.5–5 μM $NiCl_2$ up to a conductance of 600 pS [2,029 events, bin width: 5 pS, normalized to all events (2189)]. The *solid lines* are the results of fitting four Gaussian distributions (*dotted lines*) to the histograms

was performed (Fig. 2d). It is obvious that the conductance states are in the same range as those observed in the absence of Ni^{2+}. However, their distribution is significantly different. Four Gaussian functions were fitted to the data with the assumption that the mean conductance states do not change in the presence of Ni^{2+}, thus keeping these four parameters constant. The result is depicted in Fig. 2d. It is obvious that the first (131 pS) and second (181 pS) conductance levels are very prominent, while the third and fourth one are greatly diminished. The relative area of the first and second conductance state amounts to 78% in the presence and only 43% in the absence of $NiCl_2$. The goodness of the fit does not change significantly if the third conductance state (234 pS) is neglected. Fitting three Gaussian functions to the data results in $\chi^2 = 8.04$, while $\chi^2 = 7.85$ results in case of four Gaussian functions. Moreover, only 160 events were found with a conductance state above 600 pS, which is only 7% of all events that were read out compared to 21% in the absence of $NiCl_2$ (see supplementary material). Thus, we conclude that the complexation of bipyridine by Ni^{2+} results in a considerable confinement of the observed multiple conductance states. Assuming that the lowest conductance state is a result of the formation of a six-helix bundle, helix bundles with six and seven helices are preferentially formed in the presence of Ni^{2+}, whereas higher order aggregates become less likely. This considerable shift in conductance probabilities is an indication that complex formation changes the aggregation properties of the peptide helices. It has already been demonstrated that Me^{2+}-bipyridine complexes are formed if the bipyridine moiety is attached to a lipid in a membrane and is exposed to the aqueous phase (Pincus et al. 2005). Owing to steric repulsion upon formation of 1:1 complexes, dispersion of these receptor lipids in the membrane was observed. We also assume that in part 1:1 complexes are found. However, only an assembly of complexes that form conducting helix bundles can be detected by our method. An assembly of only 1:1 complexes might not be able to form stable helix bundles due to the strong electrostatic and steric repulsion. Hence, we conclude that also 1:2 and 1:3 (Ni^{2+}:bipyridine) complexes are formed in the membrane. The overall electrostatic repulsion together with the reduced diffusion rate might then prevent larger aggregates to be formed, which results in more confined conductance states.

Besides the conductance states, also the kinetics was investigated. Only events with an unambiguous transition between the closed and an open state and below 550 pS were taken for analysis. 2,992 events were subjected to a histogram analysis with a bin width of 5 ms (Fig. 3a1). The longest detectable open time was 1.54 s. 98% of all events were found in the range of 0–200 ms. A monoexponential decay function was fit to the data resulting in a rather bad accordance between data and fit. In order to elucidate whether a higher order exponential function is more appropriate, we linearized the data using a bin width of 5 ms (Fig. 3a2). Three different slopes can be identified in the graph with the corresponding open lifetimes (τ) given in the figure caption. Three τ-values were determined in the different regimes resulting in $\tau_{lin,1} = (5.8 \pm 0.3)$ ms, $\tau_{lin,2} = (16.4 \pm 0.8)$ ms, and $\tau_{lin,3} = (63 \pm 4)$ ms. Accordingly, an exponential function of third order was fitted to the histogram shown in Fig. 3a1. τ-values were obtained with $\tau_{exp,1} = (2.7 \pm 0.2)$ ms, $\tau_{exp,2} = (13 \pm 1)$ ms, and $\tau_{exp,3} = (64 \pm 20)$ ms. The duration of openings was found to be independent of the conductance levels. The observation of three different lifetimes might be a result of a different orientation of the receptor moieties, which influences the interaction of the

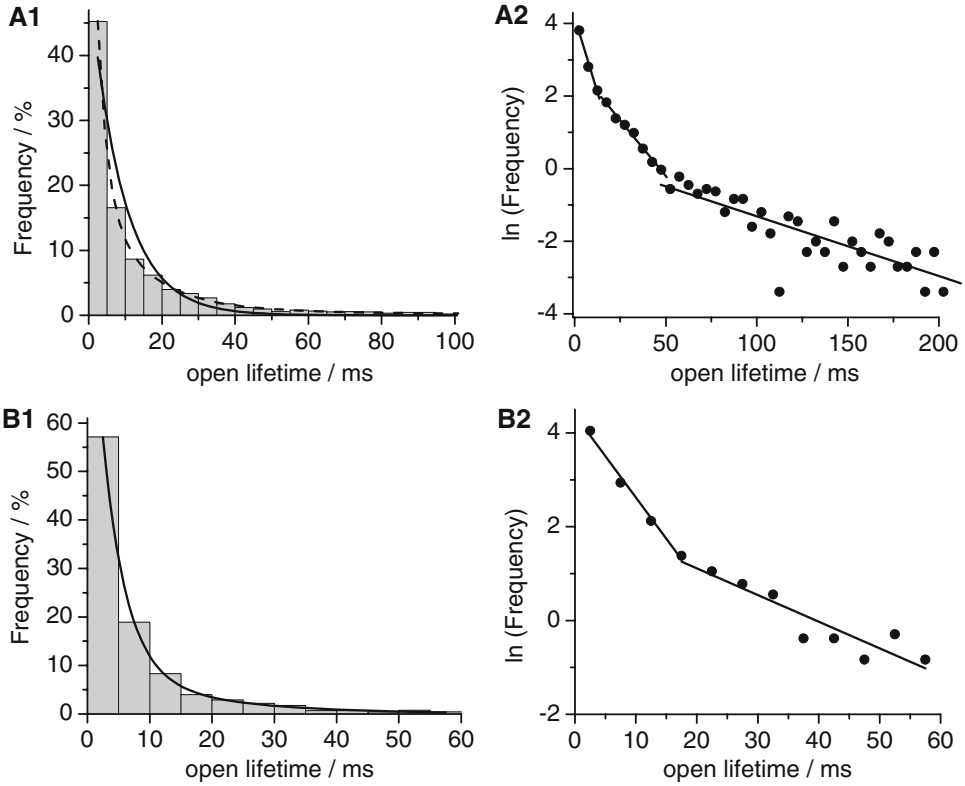

Fig. 3 Histogram analysis of the open lifetimes of **3** in nano-BLMs at +200 mV in 0.5 M KCl **a** in the absence (2,992 events) and **b** in the presence of 2.5–5 μM $NiCl_2$ (1,608 events). **a1** A monoexponential (*solid line*, $\chi^2 = 99.54$) and an exponential function of third order (*dotted line*, $\chi^2 = 0.86$) were fitted to the data with $\tau_{1,exp} = (2.7 \pm 0.2)$ ms, $\tau_{2,exp} = (13 \pm 1)$ ms, and $\tau_{3,exp} = (64 \pm 20)$ ms. **a2** Linearization of the data shown in **a1** (bin width 5 ms). The *three solid lines* show linear regressions within the corresponding data ranges resulting in $\tau_{1,lin} = (5.9 \pm 0.7)$ ms, $\tau_{2,lin} = (16.4 \pm 0.8)$ ms, and $\tau_{3,lin} = (63 \pm 8)$ ms. **b1** A biexponential function (*solid line*) was fit to the data with $\tau_{1,exp} = (3.7 \pm 0.1)$ ms, and $\tau_{2,exp} = (17 \pm 2)$ ms. **b2** Linearization of the data shown in **b1** (bin width 5 ms). The *two solid lines* show linear regressions within the corresponding data ranges resulting in $\tau_{1,lin} = (5.7 \pm 0.3)$ ms, $\tau_{2,lin} = (18 \pm 3)$ ms

peptide helices in the membrane. If the alkyl spacer with the 2,2′-bipyridine is not exposed to the aqueous phase (τ_1) but in part (τ_2), or fully (τ_3) interacts with the lipid bilayer, it is well conceivable that the diffusion of the peptide helices is diminished and hence, the helix bundle is getting more stable leading to larger open times.

To investigate the mean open lifetime of the channels in the presence of Ni^{2+}, a similar data analysis was performed (Fig. 3b). 1,608 events with an unambiguous transition between the closed and an open state below 550 pS were subjected to the histogram analysis. The longest detectable event lasted 0.57 s. Already in the time interval of 0–60 ms, 98% of all events were found. Thus, a histogram of events between 0–60 ms was plotted together with the linearized form. From the linearized data, two slopes can be identified leading to $\tau_{lin,1} = (5.7 \pm 0.3)$ ms, and $\tau_{lin,2} = (18 \pm 3)$ ms (Fig. 3b2). Fitting a biexponential decay function to the histogram (Fig. 3b1) results in $\tau_{exp,1} = (3.7 \pm 0.1)$ ms and $\tau_{exp,2} = (17 \pm 2)$ ms. Since only few events exhibited a larger open time than 60 ms, a third τ-value, similar to the one that has been found in the absence of Ni^{2+}, was not well defined. This can be explained in terms of a reduced stability of the helix bundles presumably as a result of steric repulsion due to Ni^{2+}-complexation.

In summary, the results demonstrate that the complexation of 2,2′-bipyridine functionalized amphiphathic peptides by Ni^{2+} alters the conductance behaviour of the peptides. It results in a considerable confinement of the observed multiple conductance states and diminishes the frequency of events with larger open times, while it does not change significantly the conductance levels.

Acknowledgment The authors like to thank the DFG for financial support (STE 884/4-1,2).

References

Akerfeldt KS, Lear JD, Wasserman ZR, Chung LA, DeGrado WF (1993) Synthetic peptides as models for ion channel proteins. Acc Chem Res 26:191–197

Becker CFW, Oblatt-Montal M, Kochendoerfer GG, Montal GG (2004) Chemical synthesis and single channel properties of tetrameric and pentameric TASPs (template-assembled synthetic proteins) derived from the transmembrane domain of HIV virus protein u (Vpu). J Biol Chem 279:17483–17489

Buchanan SK (1999) β-barrel proteins from bacterial outer membranes: structure, function and refolding. Curr Opin Struct Biol 9:455–461

Cafiso DS (1994) Alamethicin: a peptide model for voltage gating and protein–membrane interactions. Annu Rev Biophys Biomol Struct 23:141–165

Chung LA, Lear JD, DeGrado WF (1992) Fluorescence studies of the secondary structure and orientation of a model ion channel peptide in phospholipid vesicles. Biochemistry 31:6608–6616

Duclohier H, Alder G, Kociolek K, Leplawy MT (2003) Channel properties of template assembled alamethicin tetramers. J Pept Sci 9:776–783

Ghadiri MR, Soares C, Choi C (1992) A convergent approach to protein design. Metal ion-assisted spontaneous self-assembly of a polypeptide into a triple-helix bundle protein. J Am Chem Soc 114:825–831

Gilliam AE, Hey DH, Lambert A (1941) The absorption spectra of the phenylpyridines and pyridyldiphenyls. J Chem Soc:364–367

Gilmartin BP, McLaughlin RL, Williams ME (2005) Artificial tripeptide scaffolds for self-assembly of heteromultimetallic structures with tunable electronic and magnetic properties. Chem Mater 17:5446–5454

Gochin M, Khorosheva V, Case MA (2002) Structural characterization of a paramagnetic metal-ion assembled three stranded α-helical coiled coil. J Am Chem Soc 124:11018–11028

Gochin M, Guy RK, Case MA (2003) A metallopeptide assembly of the HIV-1 gp41 coiled coil is an ideal receptor in fluorescence detection of ligand binding. Angew Chem Int Ed 42:5325–5328

Horn C, Steinem C (2005) Photocurrents generated by bacteriorhodopsin adsorbed on nano-black lipid membranes. Biophys J 89:1046–1054

Kaes C, Katz A, Hosseini MW (2000) Bipyridine: the most widely used ligand. A review of molecules comprising at least two 2,2′-bipyridine units. Chem Rev 100:3553–3590

Kienker PK, Lear JD (1995) Charge selectivity of the designed uncharged peptide ion channel Ac-$(LSSLLSL)_3$-$CONH_2$. Biophys J 68:1347–1358

Koide T, Yuguchi M, Kawakita M, Konno H (2002) Metal-assisted stabilization and probing of collagenous triple helices. J Am Chem Soc 124:9388–9389

Lear JD, Wasserman ZR, DeGrado WF (1988) Synthetic amphiphilic peptide models for protein ion channels. Science 240:1177–1181

Liebermann M, Sasaki T (1991) Iron(II) organizes a synthetic peptide into three helix bundles. J Am Chem Soc 113:1470–1471

Mason SF (1968) The electronic spectra and optical activity of phenanthroline and dipyridyl metal complexes. Inorg Chim Acta Rev 2:89–109

Milov AD, Samiloiva RI, Tsvetkov YD, Formaggio F, Toniolo C, Raap J (2007) Self-aggregation of spin-labeled alamethicin in ePC vesicles studied by pulsed electron–electron double resonance. J Am Chem Soc 129:9260–9261

Mohler DL, Chen D, Reddy VB (2002) A facile synthesis of homologous 4,4'-dialkanoic acid substituted 2,2′-bipyridines. Synthesis 6:745–748

Montal M, Montal MS, Tomich JM (1990) Synporins-synthetic proteins that emulate the pore structure of biological ionic channels. Proc Natl Acad Sci USA 87:6929–6933

Montal MO, Iwamoto T, Tomich JM, Montal M (1993) Design, synthesis and functional characterization of a pentameric channel protein that mimics the presumed pore structure of the nicotinic cholinergic receptor. FEBS Lett 320:261–266

Mutter M, Vuilleumier S (1989) A chemical approach to protein design—template-assembled synthetic proteins (TASP). Angew Chem Int Ed 28:535–554

Pincus JL, Jin C, Huang W, Jacobs HK, Gopalan AS, Song Y, Shelnutt JA, Sasaki DY (2005) Selective fluorescence detection of divalent and trivalent metal ions with functionalized lipid membranes. J Mater Chem 15:2938–2945

Randa HS, Forrest L, Voth G, Sansom M (1999) Molecular dynamics of synthetic leucine-serine ion channels in a phospholipid membrane. Biophys J 77:2400–2410

Römer W, Steinem C (2004) Impedance analysis and single-channel recordings on nano-black lipid membranes based on porous alumina. Biophys J 86:955–965

Römer W, Lam YH, Fischer D, Watts A, Fischer WB, Göring P, Wehrspohn RB, Gösele U, Steinem C (2004) Channel activity of a viral transmembrane peptide in micro-BLMs: Vpu1-32 from HIV-1. J Am Chem Soc 126:16267–16274

Sakoh M, Okazaki T, Nagaoka Y, Asami K (2003) N-terminal insertion of alamethicin in channel formation studied using its covalent dimer N-terminally linked by disulfide bond. Biochim Biophys Acta 1612:117–121

Sansom MS (1991) The biophysics of peptide models of ion channels. Prog Biophys Mol Biol 55:139–235

Schmitt EK, Vrouenraets M, Steinem C (2006) Channel activity of OmpF monitored in nano-BLMs. Biophys J 91:2163–2171

Unwin N (2003) Structure and action of the nicotinic acetylcholine receptor explored by electron microscopy. FEBS Lett 555:91–95